Characterization of human brain nicotinamide 5′-mononucleotide adenylyltransferase-2 and expression in human pancreas

Joel A. YALOWITZ*, Suhong XIAO†, Mangatt P. BIJU†, Aśok C. ANTONY†‡, Oscar W. CUMMINGS§, Mark A. DEEG†‡ and Hiremagalur N. JAYARAM*‡[1]

*Department of Biochemistry and Molecular Biology, Richard L. Roudebush Veterans Affairs Medical Center – 151, 1481 West Tenth Street, Indianapolis, IN 46202, U.S.A., †Department of Medicine, Indiana University School of Medicine, Indianapolis, IN 46202, U.S.A., ‡Medicine Service, Richard L. Roudebush Veterans Affairs Medical Center, Indianapolis, IN 46202, U.S.A., and §Department of Pathology and Laboratory Medicine, Indiana University School of Medicine, Indianapolis, IN 46202, U.S.A.

NMNAT (nicotinamide 5′-mononucleotide adenylyltransferase; EC 2.7.7.1) catalyses the transfer of the adenylyl group from ATP to NMN to form NAD. We have cloned a novel human NMNAT cDNA, designated hNMNAT-2, from human brain. The cDNA contains a 924 bp open reading frame that encodes a 307 amino acid peptide that was expressed as a histidine-patch-containing thioredoxin fusion protein. Expressed hNMNAT-2 shared only 35 % amino acid sequence homology with the human NMNAT enzyme (hNMNAT-1), but possessed enzymic activity comparable with hNMNAT-1. Using human genomic databases, hNMNAT-2 was localized to chromosome 1q25 within a 171 kb gene, whereas hNMNAT-1 is on chromosome 1p32–35. Northern blot analysis revealed highly restricted expression of hNMNAT-2 to brain, heart and muscle tissues, which contrasts with the wide tissue expression of hNMNAT-1; different regions of the brain exhibited differential expression of hNMNAT-2. Substitution mutations of either of two invariant residues, His-24 or Trp-92, abolished enzyme activity. Anti-peptide antibody to a unique epitope within hNMNAT-2 was produced, and immunohistochemical analysis of sections of normal adult human pancreas revealed that hNMNAT-2 protein was markedly expressed in the islets of Langerhans. However, the pancreatic exocrine cells exhibited weak expression of hNMNAT-2 protein. Sections of pancreas from insulinoma patients showed strong expression of hNMNAT-2 protein in the insulin-producing tumour cells, whereas acinar cells exhibited relatively low expression of hNMNAT-2 protein. These data suggest that the unique tissue-expression patterns of hNMNAT-2 reflect distinct functions for the isoforms in the regulation of NAD metabolism.

Key words: enzyme kinetics, human NMN adenylyltransferase, immunohistochemistry, NAD metabolism, protein expression, protein purification.

INTRODUCTION

NMNAT (nicotinamide 5′-mononucleotide adenylyltransferase; EC 2.7.7.1) is the key enzyme of NAD^+ synthesis in a pathway conserved across many lifeforms [1]. NMNAT catalyses the addition of adenylate from ATP to NMN or nicotinic acid mononucleotide, forming NAD^+ or nicotinic acid adenine dinucleotide, which is then converted to NAD^+ by NAD^+ synthase (EC 6.3.1.5). NAD^+ and its phosphorylated derivative $NADP^+$ are used reversibly in catabolic reactions such as glycolysis, fatty acid oxidation, nitrogen metabolism, one-carbon metabolism, and in anabolic reactions such as gluconeogenesis, and fatty acid, amino acid, cholesterol and nucleotide synthesis. NAD^+ has been shown to be necessary for cell survival in oxidative stress and DNA damage.

Tiazofurin (2-β-D-ribofuranosylthiazole-4-carboxamide) is an anti-cancer prodrug that inhibits inosine-5′-monophosphate dehydrogenase only after it is anabolized intracellularly to its monophosphate and then to its active form, TAD (thiazole-4-carboxamide adenine dinucleotide), an analogue of NAD, by NMNAT [2]. TAD binds to the NAD^+ half-site of inosine-5′-monophosphate dehydrogenase. hNMNAT-1 (human NMNAT-1) was co-crystallized with a non-hydrolysable analogue of TAD, β-methylene-TAD [3]. Tiazofurin sensitivity is primarily a function of NMNAT activity, and resistant cell lines show decreased NMNAT activity [4]. Thus the relative activity of NMNAT in various tissues will influence the effect of tiazofurin activation in those tissues; this in turn will be relevant to the use of tiazofurin as an anti-cancer agent and provide insight into tissue-specific toxicity. Because a consistent side effect of tiazofurin was somnolence and in some cases seizures during our phase I/II trial [5], it suggested that TAD could be formed in the brain by hNMNAT.

NMNAT has been purified from human placenta [6], yeast [7–9] and other micro-organisms [10–15]. Two genes, *YLR328W* and *YGR010W*, coding for yeast NMNAT were cloned [8,9]. Human NMNAT, termed hNMNAT-1, as well as mouse NMNAT (with 64 % identity to hNMNAT-1) was recently cloned and crystallized [3,11,16–23] and shown to be localized in the nucleus. Although Northern blot analysis showed that hNMNAT-1 is expressed in heart, muscle, liver, kidney and pancreas with variable intensity [11], a signal was barely detectable in human brain. Nevertheless, due to the requirement for consistent levels of NAD^+ in tissues such as heart and nervous system, especially during hypoxic injury [24], and the neurological effects of tiazofurin analogues, it appeared reasonable to hypothesize the existence of a tissue-specific form of NMNAT in human brain. Accordingly, we determined whether a second brain-specific human NMNAT existed. During preparation of this article, another group reported the cDNA of a second hNMNAT specific to human brain [25]. Here we describe briefly our molecular and site-directed mutagenesis studies and compare the expression of hNMNAT-2 in human pancreas and insulinoma. Our studies suggest that cell-specific

Abbreviations used: EST, expressed sequence tag; NMNAT, nicotinamide mononucleotide adenylyltransferase; hNMNAT, human NMNAT; RT-PCR, reverse transcriptase–PCR; TAD, thiazole-4-carboxamide adenine dinucleotide; IDDM, insulin-dependent diabetes mellitus.

[1] To whom correspondence should be addressed, at the Department of Biochemistry and Molecular Biology (e-mail hjayaram@iupui.edu).

and tissue-specific expression of hNMNAT-2 in human pancreas probably reflect a physiological function.

EXPERIMENTAL

Materials

All reagents were obtained from Sigma (St. Louis, MO, U.S.A.) and were of the highest available purity. Oligonucleotide primers were synthesized by Gibco/Invitrogen (Carlsbad, CA, U.S.A.). The random hexanucleotide primer kit for generation of radiolabelled DNA probes was from Stratagene (La Jolla, CA, U.S.A.). [α-^{32}P]dCTP (specific activity >1000 Ci/mmol) was from Amersham Biosciences (Arlington Heights, IL, U.S.A.). Human multiple-tissue blot was from Origene (Rockville, MD, U.S.A.). *Taq* polymerase was from Perkin-Elmer (Boston, MA, U.S.A.) and *Pfu* polymerase was from Promega (Madison, WI, U.S.A.). Expand Long Template polymerase mix was from Roche (Indianapolis, IN, U.S.A.). The cDNA clone EST26487 was obtained from the American Type Tissue Collection (Manassas, VA, U.S.A.). pTrcHisTOPO-TA and pBAD/Thio-TOPO vectors were obtained from Invitrogen. DNA sequencing was performed using a Perkin-Elmer-ABI 377XL DNA sequencer using Perkin-Elmer Big Dye chemistry.

Cloning of hNMNAT-2

Two ESTs (expressed sequence tags) termed C1ORF15 and KIAA0479 (GenBank accession numbers AAG60615 and BAA-32324) [26–28] were identified during a BLAST search for homologues of the recently cloned yeast NMNAT gene YLR328W (GenBank accession number AAB64524). Several identical cDNA sequences were recognized that were all cloned from human nervous tissue sources (infant brain, fetal cochlea, cerebellum and neuroepithelium). The KIAA0479 human cDNA encoded a 5439 nucleotide transcript containing a 307 amino acid open reading frame beginning from the first initiation codon. The C1ORF15 cDNA was 5691 nucleotides in length and possessed a 5′ extension of 112 nucleotides. This extended 5′ region contained three stop codons in frame with the open reading frame, suggesting that the open reading frame was complete and not a 3′ fragment from a longer open reading frame. The KIAA0479 cDNA was obtained as a T. I. G. R. EST (EST26487) [26]. The open reading frame was cloned by PCR amplification using *Pfu* polymerase and the primers EST-ORF-FWD (5′-ATG ACC GAG ACC ACC AAG AC-3′), and EST-NCO-3′ (5′-CGA ACC ATG GAC TAG CCG GAG GCA TTG ATG-3′). A single fragment of approx. 924 bp was amplified and cloned into the pTrcHisTOPO-TA and pBAD/Thio-TOPO vectors. Clones were sequenced to verify accuracy.

Enzyme activity

Purified protein (described below) was analysed for NMNAT activity by continuously coupled NMNAT and alcohol dehydrogenase reactions with product formation observed by absorbance at 340 nm as described in [29]. Briefly, 1.5 ml of enzyme master mix contained 360 μl of 100 mM Hepes, pH 7.5, containing 40 mM $MgCl_2$, 30 μl of 120 mM neutralized ATP (pH 7.6), 15 μl of 60 mM NMN, 75 μl of yeast alcohol dehydrogenase (0.5 mg/ml), 585 μl of 35 mM semicarbazide, pH 7.5, 7.5 μl of ethanol, and the balance enzyme and water. Reactions were carried out at 37 °C, and read in a 1 ml, 1 cm-light-path cuvette at 340 nm. Control reactions served as references. One unit of activity is defined as the amount that synthesized 1 μmol of NAD^+/min. An NADH molar absorption coefficient of 6220 $M^{-1} \cdot cm^{-1}$ was used. Unless otherwise specified, all kinetic experiments were performed in triplicate.

Expression and purification of hNMNAT-2

hNMNAT-2 was expressed using the plasmids pTrcHisTOPO-TA and pBAD/Thio-TOPO in separate experiments. NMNAT enzyme activity was followed during each step of the purification scheme. Proteins were expressed in *Escherichia coli* TOP10 cells (Invitrogen) in LB broth containing 100 mg/l ampicillin and induced with 1 mM isopropyl β-D-thiogalactoside (pTrcHisTOPO-TA) or 0.2 % arabinose (pBAD/Thio-TOPO). Cells were grown to late log phase and induced, then harvested by centrifugation. Cells were lysed using a French pressure cell at 2200 psi (15180 kPa) in 100 mM potassium phosphate, pH 7.6, containing 1 μM PMSF and 1 mg/ml benzamidine. hNMNAT-2 protein was purified using Qiagen Ni^{2+}-nitrilotriacetate immobilized metal-affinity chromatography. Briefly, protein was loaded in lysis buffer containing 1 mM histidine, washed with 100 mM potassium phosphate, pH 7.6, containing 5 mM histidine, and eluted with a linear gradient from 5 to 100 mM histidine in 100 mM potassium phosphate, pH 7.6. hNMNAT-2 protein was stored at 4 °C during analysis and at -20 °C in 50 % glycerol for long-term storage. hNMNAT-2 protein stored at 4 °C for 2 days showed 90 % of original activity, and 50 % activity after 1 week.

Site-directed mutagenesis

Site-directed mutagenesis was carried out using whole plasmid synthesis [30]. For whole plasmid synthesis, oligonucleotides containing point mutations in one of two conserved residues (His-24 and Trp-92) were used for long-template PCR on hNMNAT-2-containing clones using Expand Long Template polymerase. Resulting reactions were digested with *Dpn*I to eliminate bacterially derived template DNA. Site-directed mutagenesis introduced a unique restriction site that was used for restriction endonuclease analysis of the products to ensure the presence of the mutation, and confirmed by sequencing. Plasmids were cloned and expressed as above. Oligonucleotide primers were H24A-FWD (5′-CCC ATC ACC AAA GGG CCC ATT CAG ATG TTT GAA-3′) and its complement H24A-REV, and W92G-FWD (5′-TGC TAC CAG GAC ACC GGT CAG ACG ACC TGC AGC-3′) and its complement W92G-REV.

Protein analysis

Purity was evaluated by SDS/PAGE analysis and Coomassie Blue staining. Protein concentrations were determined by the method of Bradford and Lowry (Bio-Rad, Hercules, CA, U.S.A.) [31].

Northern blot analysis

The Origene Multiple Choice human multiple tissue Northern blot contained 2 μg of poly(A)$^+$ RNA from the following human tissues: brain, colon, heart, kidney, liver, lung, muscle, placenta, small intestine, spleen, stomach and testis. A probe was generated to a 751 nucleotide region immediately 3′ of the coding sequence of the cloned cDNA (nucleotides 2010–2761). The probe was amplified by PCR using primers hNMNAT-2-3P-FWD (5′-TGA TGG CAC AGT GCG GGT-3′) and -REV (5′-ACC TGG CCC TTT CTG GCC-3′) and labelled with [α-^{32}P]dCTP by

random hexamer labelling. Prehybridization and hybridization were carried out at 68 °C using ExpressHyb solution (Clontech). Following hybridization for 18 h and washing, the blot was exposed to Kodak Biomax film at −80 °C for 24 h. RNA integrity and loading was assessed using a human β-actin probe. A human brain multiple-tissue Northern blot was obtained from Clontech (human brain MTN II). The blot contained 2 μg of poly(A)$^+$ RNA from the following human tissues: cerebellum, cerebrum, medulla, spinal cord, occipital lobe, frontal lobe, temporal lobe and putamen. The blot was hybridized in the same fashion with the same probe.

RT-PCR (reverse transcriptase–PCR)

Total RNA was isolated from 2×10^7 cells (Trizol; Gibco, Bethesda, MD, U.S.A.). cDNA was synthesized using oligo-dT primers (Superscript II first-strand cDNA synthesis kit; Gibco) in a 50 μl total volume. We used 1 μl of the total cDNA per RT-PCR reaction. Primers used were EST-ORF-FWD and EST-NCO-3′, as above; hNMNAT-2-3P-FWD and -REV, as above; hNMNAT-2-266-FWD (5′-GAA AAC AGG GCC TCG TG-3′); hNMNAT-2-565-FWD (5′-GTG GGA GAA AGC CTC AG-3′); hNMNAT-1-FWD (5′-CTT ACC ATG GAA AAT TCC-3′) and hNMNAT-1-REV (5′-TG TCT TAG CTT CTG CAG TG-3′). Each reaction (12 μl) was run on a 1 % agarose gel containing ethidium bromide.

Genomic analysis of hNMNAT-2

Genomic DNA databases were searched using BLAST and viewed using Ensemble. hNMNAT-2 matched several sequences in both draft and completed contigs. Completed contigs were used to define the genomic organization of the gene, as draft sequences were found to be incorrectly ordered and oriented. Three overlapping completed genomic contigs on chromosome 1q25 contained the entire hNMNAT-2 sequence. Exons were found to cover the complete hNMNAT-2 mRNA sequence. GenBank accession numbers for genomic clones were AL354953, AL356981 and AL449223.

Peptide synthesis and antibody production

Peptide sequence unique for hNMNAT-2 (GKVGESLSRIC-CVRPPVERFTFVD) was selected and synthesized by the solid-phase method using Fmoc (fluorenylmethoxycarbonyl)/tertiary butyl chemistry on an Applied Biosystems model 433 automated synthesizer. The peptide sequences were verified by matrix-assisted laser-desorption ionization MS. Rabbit polyclonal purified IgG antibodies were raised from hNMNAT-2 peptide by Strategic Biosolutions (Newark, DE, U.S.A.).

Immunohistochemistry procedures

Adult human normal pancreas and insulinoma tissue slides were obtained from the Indiana University Cancer Center Tissue Bank. The insulinomas had been characterized clinically by serum insulin levels prior to their resection. The slides were fixed with 10 % buffered formalin (Sigma) at 25 °C for 48 h, washed twice with PBS without calcium and magnesium, pH 7.4 (Gibco/BRL, Grand Island, NY, U.S.A.), and processed in an automatic tissue processor Leica TP 1020 (Leica Microsystems, GmBH, Mannheim, Germany) under vacuum. For immunohistochemical staining of hNMNAT-2 proteins, the slides were incubated at 70 °C for 1 h and deparaffinized by washing with xylene. Sections were then stepwise rehydrated in ethanol from 100 to 70 % and washed with water. The sections were microwaved for 20 min at 90 % power in citrate buffer (pH 6.0) for antigen retrieval. Endogenous peroxidase activity was suppressed by immersing sections in 0.3 % H_2O_2/methanol for 30 min at 22 °C. After processing with the Vector blocking kit (Vector Laboratories, Burlingame, CA, U.S.A.), sections were blocked in 10 % (v/v) normal goat serum in PBS for 60 min and then incubated with primary rabbit anti-hNMNAT-2 peptide IgG or non-immune rabbit serum IgG (1:800 in 2 % normal goat serum) overnight at 4 °C. After washing in PBS, sections were processed using a Vectastain Elite avidin-biotin peroxidase kit (Vector Laboratories) with DAB (diaminobenzidine) as the chromogen/substrate. Sections were washed, then dehydrated with ethanol followed by xylene, and mounted with Permount (Fisher, Pittsburgh, PA, U.S.A.). Images were captured with either a Leica MZAPO dissecting microscope or a Leitz DMLB light microscope equipped with a Diagnostic Instruments Spot digital camera and processed using Adobe Photoshop software. Control experiments verified that specific immunostaining did not occur in the absence of primary antibodies.

Other methods

Database searching was carried out using BLAST [29] and alignment generation was performed using EMBnet and PISE [32]. Statistical analysis was carried out using Microsoft Excel. Enzyme kinetic calculations were performed using nonlinear analysis [33]. The phylodendrogram was produced using Treeview, written by R. D. M. Page [34].

RESULTS

Primary sequence analysis

The known yeast NMNAT protein sequence YLR328W was used to probe the NCBI database using BLAST searching. The sequence of the open reading frame encoded by KIAA0479 and C1ORF15 demonstrated moderate homology with YLR328W. KIAA0479 and C1ORF15 share the same coding sequence of the open reading frame, but differ by a 4 nucleotide deletion in the non-coding sequence. KIAA0479 has an ambiguous 5′ terminus, with no in-frame stop codon upstream of the open reading frame. C1ORF15 is an identical sequence with a 5′ extension showing three in-frame stop codons upstream of the open reading frame (results not shown). In addition, the initiation codon is within a favourable Kozak sequence (ACCATGA) [35] and is the highest-scoring initiation codon in the cDNA sequence [7]. Therefore, the open reading frame encoded by the genes was assumed to be complete. This open reading frame was amplified by PCR and directly cloned.

Two cDNA sequences entitled hNMNAT-2 variants 1 and 2 were recently deposited in the GenBank database. The variant 1 cDNA differs from the C1ORF15 sequence only in the downstream non-coding sequence: hNMNAT-2 variant 1 has a total of three deletions ranging from 1 to 6 nucleotides. Analysis of the two cDNA sequences shows that variant 2 has a different 5′ end of about 270 nucleotides. hNMNAT-2 variant 2, however, encodes a different open reading frame, encoding a hypothetical protein with a different N-terminal sequence, including the consensus amino acid His-24 (altered to Phe in variant 2). The novel 5′ terminus of the variant 2 cDNA appears to match a genomic sequence upstream of the 5′ terminus of the C1ORF15/KIAA0479

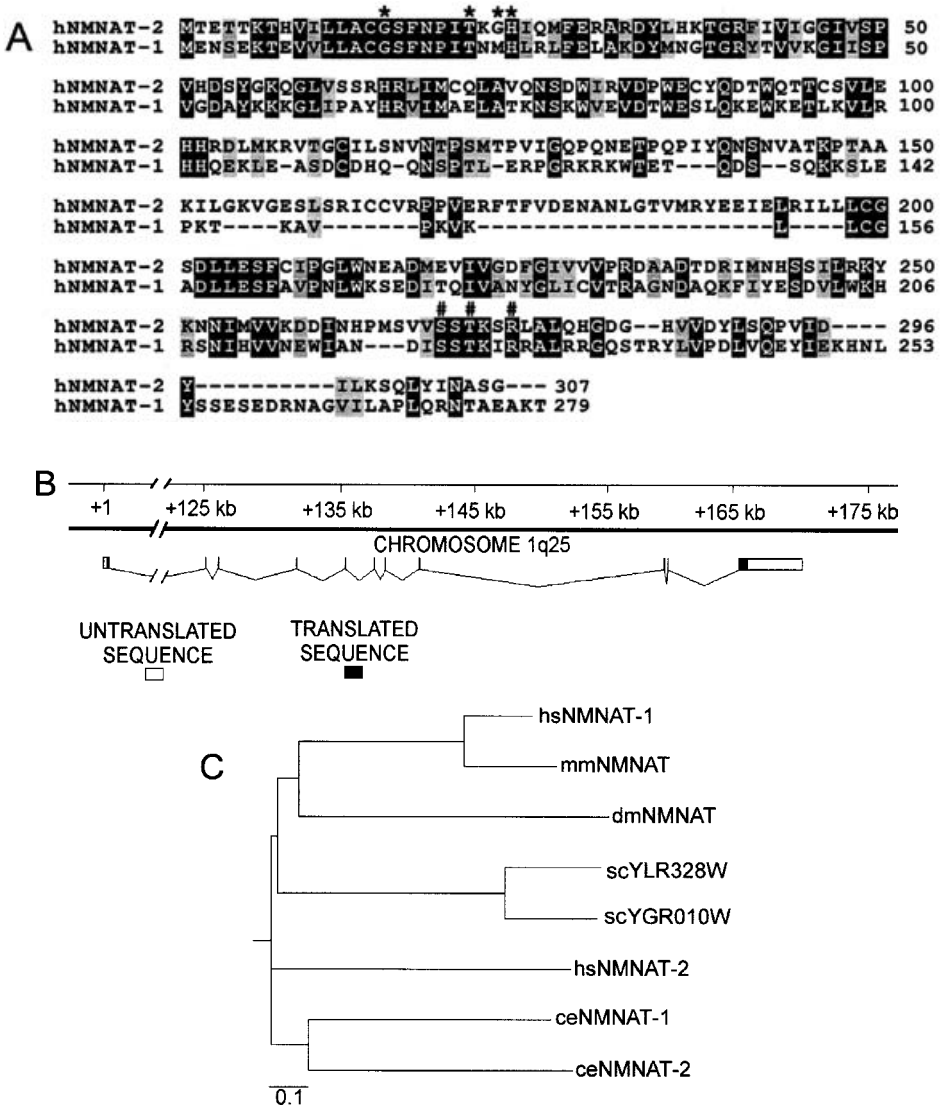

Figure 1 hNMNAT-2 protein sequence, genomic organization and phylogeny of eukaryotic NMNATs

(**A**) hNMNAT-2 primary sequence was aligned with hNMNAT-1 sequence using ClustalW. The sequences show 35 % identity. Black boxes indicate identical residues; grey boxes indicate conserved substitutions; asterisks (*) indicate N-terminal residues conserved among NMNAT enzymes; # indicate conserved C-terminal residues. (**B**) Genomic organization of hNMNAT-2. Shown is a schematic of the 171 kb region of chromosome 1q25 containing the cDNA, present in 11 exons. (**C**) Dendrogram of eukaryotic NMNAT genes. Protein sequences of known eukaryotic NMNAT genes were aligned. Bar indicates a 0.1 fractional difference in sequence alignment. hs, *Homo sapiens*; mm, *Mus musculus*; dm, *Drosophila melanogaster*; sc, *Saccharomyces cerevisiae*; ce, *Caenorhabditis elegans*.

transcript, raising the possibility of an alternative transcription start site.

Although the sequences of the hNMNAT-1 [11] and hNMNAT-2 exhibited significant divergence, they matched in two areas of consensus among all known NMNATs. Figure 1(A) shows the amino acid homology between hNMNAT-2 and hNMNAT-1. hNMNAT-2 shows 35 % sequence identity with hNMNAT-1 (black boxes) and numerous conserved substitutions (grey boxes). Two consensus sequences common to all observed NMNATs (from human, mouse, yeast and several prokaryotes) have been described: an N-terminal motif present in α/β nucleotidyltransferases [GXXXPX(T/H)XXH] and a C-terminal motif SXTXXR [36]. Both sequences were present in hNMNAT-2: G^{15}SFNPITKGH^{24} in the N-terminus (designated by asterisks in Figure 1A) and S^{269}STKSR^{274} in the C-terminus (designated by # in Figure 1A). hNMNAT-2 lacked a nuclear localization signal, transmembrane domains and a signal peptide. Using computer-based protein search algorithms for localization signals [37], hNMNAT-2 was predicted to localize to the cytoplasm. This contrasts with hNMNAT-1 and mouse NMNAT that are localized to the nucleus.

The genomic organization of hNMNAT-2 is shown in Figure 1(B). The predicted mRNA appears on chromosome 1q25 in 11 exons, accounting for the entire mRNA represented by C1ORF15/KIAA0479. The final exon is large (4508 nucleotides) while the first 10 exons are short (48–420 nucleotides in length). The entire gene covers approx. 171 kb with a very large first intron (approx. 125 kb). A TATA box with the sequence GAAATAAACA was detected at position −219 by a computer-based algorithm [38]. The gene ends with a polyadenylation signal (AAUAAA) 12 nucleotides from the end of the cDNA. Several more polyadenylation signals appear throughout the gene but only

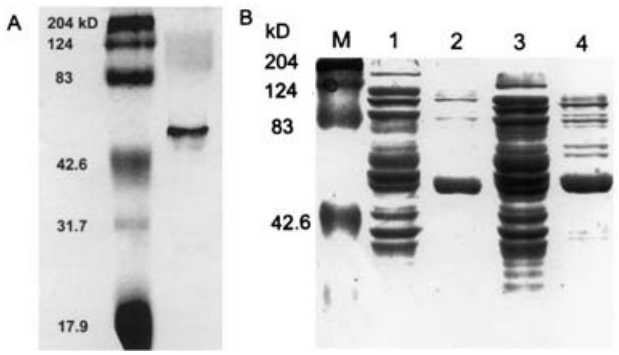

Figure 2 Purified hNMNAT-2 fusion proteins

(**A**) SDS/PAGE analysis of purified hNMNAT-2 fusion protein. A 12 % acrylamide gel was loaded with 50 μg of protein and stained with Coomassie Brilliant Blue. Left-hand lane, polypeptide standards labelled with their molecular mass in kDa; right-hand lane, purified hNMNAT-2. The apparent molecular mass of hNMNAT-2 is 50 kDa due to the thioredoxin tag. (**B**) SDS/PAGE analysis of crude and purified mutant proteins, stained with Coomassie Brilliant Blue. M, molecular mass markers; lane 1, crude lysate of *E. coli* overexpressing H24A-mutant hNMNAT-2; lane 2, purified product from lane 1; lane 3, crude lysate of *E. coli* overexpressing W92G-mutant hNMNAT-2; lane 4, purified product from lane 3.

the last one is followed by a canonical GUGU-rich sequence. Coding begins within exon 1 and ends on exon 11, followed by a 3′-untranslated region. The gene is positioned next to the LAMC2 gene (laminin γ2) in a 3′-to-3′ orientation.

Figure 1(C) presents a dendrogram of observed eukaryotic NMNAT sequences. hNMNAT-2 exhibited significant divergence from hNMNAT-1, which actually shares more homology with mouse NMNAT (61 % identity) than with hNMNAT-2 (35 % identity). hNMNAT-2 is somewhat more homologous with the theoretical *Caenorhabditis elegans* NMNAT enzymes than with hNMNAT-1. The yeast NMNAT sequences are closely related to one another (77 % identity) but highly divergent from other eukaryotic sequences. When aligned with prokaryotic NMNAT sequences, hNMNAT-2 showed low sequence homology (10–18 % across several species; results not shown).

Expression, purification and properties of hNMNAT-2

The human brain NMNAT-2 cDNA was cloned into prokaryotic expression vectors, with the first initiation codon used as the protein start site. The encoded protein has a theoretical molecular mass of 34.4 kDa and pI of 6.59. Because nickel-affinity chromatography resin failed to bind the 6 × His-tagged protein, HisPatchThioFusion (histidine-patch-containing thioredoxin)-tagged fusion proteins were generated. HisPatchThioFusion-tagged hNMNAT-2 proved amenable to nickel-affinity purification, and NMNAT enzymic activity was robust. A single step of nickel-affinity chromatography yielded an increase in specific activity from 0.28 units/mg in the crude to 13.0 units/mg in the nickel-affinity chromatography eluate with a 28 % recovery of total activity. A histidine gradient elution proved to yield the highest purity enzyme. The purified fusion protein appeared as a single band on Coomassie Blue stained SDS/PAGE (Figure 2A). The apparent molecular mass of 50 kDa was expected due to the 13 kDa N-terminal and 3 kDa C-terminal tags contributed by the fused polypeptide.

The purified fusion protein was characterized kinetically, and forward-reaction kinetic parameters are presented in Table 1. The influence of pH on enzyme activity demonstrates a broad pH optimum, covering pH 5.6–8.5 (results not shown). This is in agreement with published data using purified human placental NMNAT and recombinant hNMNAT-1. The hNMNAT-2 fusion protein has a specific activity of 13.0 units/mg, compared with 51.0 units/mg for hNMNAT-1. The substrate affinities of hNMNAT-2 and hNMNAT-1 are similar, with K_m values of 30 and 23 μM for NMN and of 107 and 36 μM for ATP, respectively. The influence of metal cations on the enzyme activity of the hNMNAT-2 fusion protein, compared with published values for hNMNAT-1, is shown in Table 2. Metal requirements were also found to be similar to hNMNAT-1 [11], in that a bivalent metal was required for activity. Whereas 5 mM magnesium and manganese supported equivalent activities, nickel and calcium supported partial activity at equivalent concentrations, while tin and zinc supported no activity.

Table 1 Comparison of the kinetic properties of purified recombinant hNMNAT-2 with those of hNMNAT-1

One unit of activity is defined as that which synthesizes 1 μmol of NAD^+/per min at 37 °C. NR, not reported. Data for hNMNAT-1 are from [11].

Variable	hNMNAT-2	hNMNAT-1
Specific activity*†	13.0 ± 0.6 units/mg	51 units/mg
V_{max}/K_m, NMN*†	536 ± 21 μmol/min per mg	2217 μmol/min per mg
V_{max}, NMN*	11.4 ± 0.29 units/mg	NR
K_m, NMN*	30 ± 4.4 μM	23 μM
V_{max}, ATP†	11.56 ± 0.48 units/mg	NR
K_m, ATP†	107 ± 20 μM	36 μM
pH optimum*†	5.6–8.5	6.0–8.0

* At saturating conditions of ATP (2.5 mM).
† At saturating conditions of NMN (0.6 mM).

Table 2 Comparison of the influence of bivalent metals on the activity of hNMNAT-2 fusion protein with that of hNMNAT-1

Relative activity is at saturating concentrations of ATP and NMN. Data for hNMNAT-1 are from [11]. NR, not reported; ND, not done.

	hNMNAT-2		hNMNAT-1	
Divalent metal	Concentration (mM)	Relative activity (%)	Concentration (mM)	Relative activity (%)
None	0	0		
Mg^{2+}	5	100	12	100
Mn^{2+}	5	95	6	58
Ca^{2+}	5	30	NR	ND
Ni^{2+}	5	20	1	83
Zn^{2+}	5	0	0.3	63
Sn^{2+}	5	0	NR	ND

Generation and analysis of mutant hNMNAT-2 enzymes

Site-directed mutagenesis was employed to mutate consensus residues of the hNMNAT-2 protein to determine their requirement for enzymic activity. Point mutations were generated to two invariant residues in the N-terminus: His-24 was mutated to Ala (H24A), and Trp-92 was mutated to Gly (W92G). Proteins were purified by nickel-affinity chromatography in the same fashion as wild-type proteins. Figure 2(B) shows SDS/PAGE analysis of crude extracts and purified proteins. Densitometric analysis of the protein gel indicated that H24A was increased from 20.1 % purity in crude extract to 80.1 % purity (Figure 2B, lanes 1 and 2), and W92G was increased from 16.6 to 55.4 % purity (Figure 2B, lanes 3 and 4).

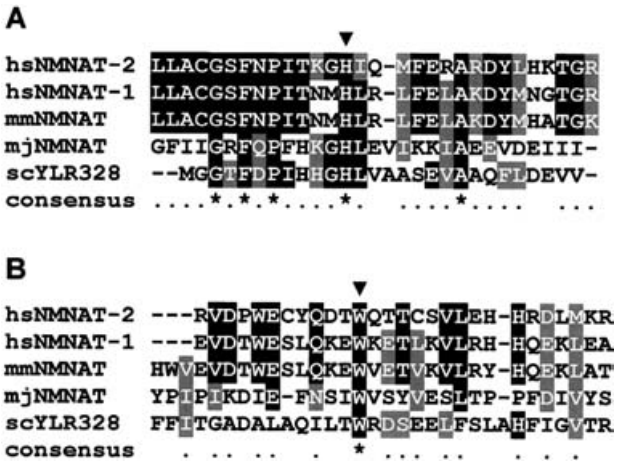

Figure 3 Comparative sequences of hNMNAT-2 mutant enzymes, and their alignment with known NMAT enzymes cloned from other species

Multiple sequence alignments are shown of the two hNMNAT-2 mutant enzymes that were generated. Alignments with known NMNAT enzymes cloned from other species indicate the conserved nature of the residues mutated. The arrowheads above the sequences indicate the mutated residues. (**A**) H24A-mutant hNMNAT-2; (**B**) W92G-mutant hNMNAT-2. hs, *Homo sapiens*; mm, *Mus musculus*; mj, *Methanococcus jannaschii*; sc, *Saccharomyces cerevisiae*.

Figure 3 shows amino acid sequence alignments of several eukaryotic and prokaryotic NMNAT enzymes, illustrating the conserved residues targeted for mutagenesis in the present study (arrowheads). The invariant residues are present in sequences as distantly related to humans as the archaebacterium, *Methanococcus jannaschii*. Proteins expressed from both mutant constructs were greatly reduced in activity compared with the wild-type protein (< 5 %; results not shown). This confirmed that highly conserved residues within NMNAT are essential for enzymic activity.

Northern blot analysis of the expression of hNMNAT-2

The expression of hNMNAT-2 was determined by Northern blot analysis (Figure 4A) using a 751 nucleotide probe derived from the cDNA sequence, beginning approx. 700 nucleotides downstream of the open reading frame to ensure maximal specificity. The results demonstrated an apparently restricted pattern of mRNA expression in brain, heart and muscle. A prominent band of 5.6 kb was noted in all three tissues, corresponding to the cloned hNMNAT-2 cDNA, which was 5.4 kb. A smaller, more abundant transcript of approx. 3.2 kb was noted in skeletal muscle; the significance of this smaller transcript is unknown. Very faint bands in the brain tissue and other broad bands that appeared ubiquitously are likely to be non-specific hybridization products. By contrast, hNMNAT-1 is expressed in heart, skeletal muscle, liver, kidney and pancreas when examined by multiple-tissue Northern blotting, and detected at very low levels in brain [11].

To more accurately define the expression of hNMNAT-2 in brain, a human brain multiple-tissue Northern blot was hybridized with the same hNMNAT-2 probe (Figure 4B). The blot showed that many tissues of the human central nervous system expressed hNMNAT-2 highly as a single band: whole cerebrum, cerebellum, occipital, frontal and temporal lobe cortices, and the putamen. The medulla showed only minimal expression, while none was detectable in the spinal cord.

The expression of hNMNAT-2 was determined in three human cell lines by qualitative RT-PCR. Figure 5 shows results repre-

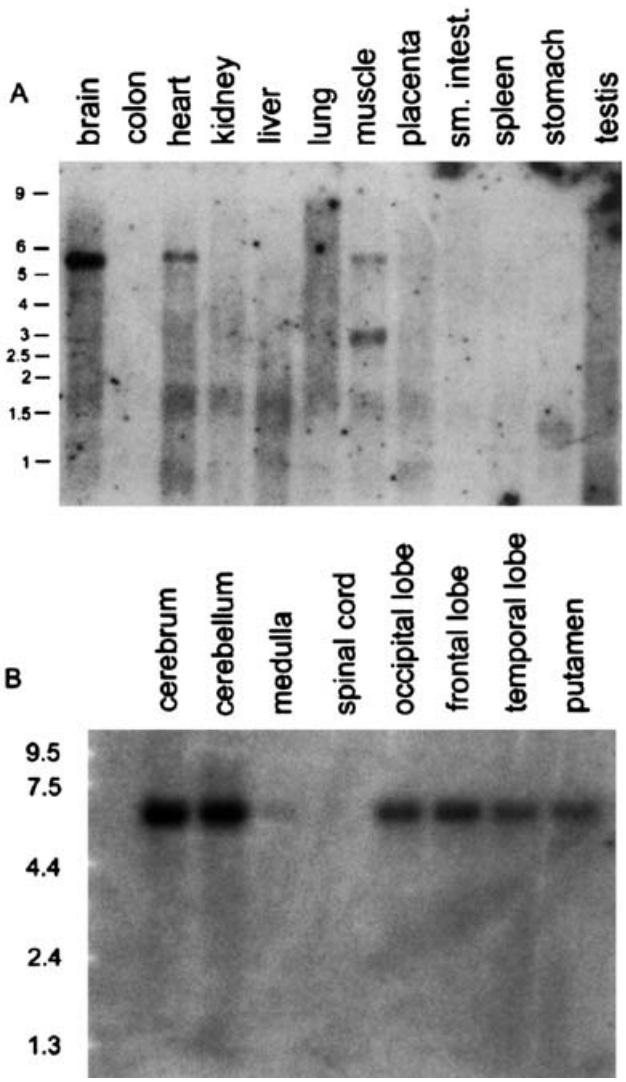

Figure 4 Northern blot analysis of the expression of hNMNAT-2

Human multiple-tissue (**A**) and brain (**B**) Northern blots containing 2 μg of poly(A)$^+$ RNA/lane were hybridized using a radiolabelled hNMNAT-2-derived probe (2010–2761 bp in the cDNA sequence). Transcript size in kb is shown on the left.

sentative of five separate experiments. K562 erythroleukaemia and HT-29 and Caco-2 colon adenocarcinoma lines were used since they are sensitive to tiazofurin due to their high NMNAT activity. Amplification of hNMNAT-1 was also performed as a control, since hNMNAT-1 is known to be expressed in several normal tissues and cell lines [11]. No amplification was seen using hNMNAT-2 (Figure 5, lanes 1–5), whereas hNMNAT-1 was amplified in all three cell lines (Figure 5, lanes 6–10). To ensure that the absence of hNMNAT-2 from the cell lines was valid, amplification of 3′ fragments of the cDNA open reading frame beginning at bp 266 and 565 was also attempted, as well as amplification of the probe sequence, approx. 700 bp downstream of the open reading frame. All results for hNMNAT-2 were negative, whereas all attempts to amplify hNMNAT-1 by RT-PCR were successful (results not shown).

Immunohistochemcal studies

Environmental agents or reactive oxygen species generated by inflammatory reactions are known to cause pancreatic β-cell death

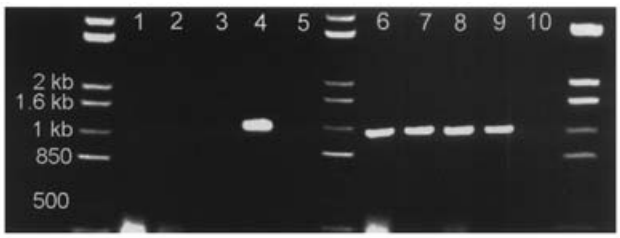

Figure 5 RT-PCR analysis of the expression of hNMNAT-2 in human cancer cell lines

RT-PCR was performed to determine expression in human cell lines. The results were run on a 1 % agarose gel stained with ethidium bromide. Cloned plasmid DNA (0.1 ng) containing the appropriate cDNA was used as a positive control. Lanes 1–5 are RT-PCR using primers for hNMNAT-2; lanes 6–10 are RT-PCR using primers for hNMNAT-1. Lanes 1 and 6, K562 cells; lanes 2 and 7, HT-29 cells; lanes 3 and 8, Caco-2 cells; lanes 4 and 9, positive control; lanes 5 and 10, negative control. The figure is representative of five experiments.

resulting in IDDM (insulin-dependent diabetes mellitus; also known as Type I diabetes) [39]. IDDM can be induced in rodents by injecting streptozotocin [2-deoxy-2-(3-methyl-3-nitrosourea)1-D-glucopyranose] and this results in rapid depletion of NAD in islet cells [40], which can be prevented by injection of nicotinamide immediately before or soon after the administration of streptozotocin [41]. Streptozotocin, a nitrosourea analogue of glucose, is shown to induce DNA strand breaks activating PARP [poly(ADP-ribose)polymerase], which utilizes NAD as its only substrate leading to a rapid reduction in NAD levels in the isolated pancreatic islets *in vitro*. NAD depletion also leads to reduction in ATP levels and ultimately to β-cell death [42,43]. Hence, it was of importance to examine by immunohistochemical analysis the expression of hNMNAT-2 in the human pancreas and to compare its expression in insulinoma tumours, wherein there is proliferation of insulin-producing β-cells.

Towards this goal, polyclonal anti-peptide antibodies were generated against an hNMNAT-2 peptide which did not share homology with any other unrelated protein in available databases by BLAST analyses. All immunohistochemical studies were performed at the same dilutions of 1:800 for anti-hNMNAT-2 antibodies to determine if there was a qualitative difference in expression in sections of human pancreas. Sections of normal adult human pancreas showed weak cytoplasmic expression of hNMNAT-2 proteins in exocrine parenchymal cells (Figure 6A). In contrast, there was marked expression of hNMNAT-2 in the islets of Langerhans, in the human pancreas, predominantly in the cytoplasm. The staining was not uniform throughout the islet, but there was more intense staining in some cells at the periphery of the islet. In sections taken from the pancreas of insulinoma patients (Figures 6C, 6E and 6G), expression was relatively uniform throughout the cytoplasm but was also observed in the nucleus. In essence, the sections taken from three patients with clinically diagnosed insulinoma showed strong expression of hNMNAT-2 protein in the insulin-producing tumour cells, whereas acinar cells exhibited relatively weak expression of hNMNAT-2 protein.

DISCUSSION

Our studies on human brain hNMNAT-2 cDNA gave similar results to a recently published study [25]. Human hNMNAT-2 had similar enzyme activity as hNMNAT-1 despite sharing only 30 % sequence homology with hNMNAT-1 [11]. Although many of the kinetic features described here were similar to those in the recent report [26] we found broad pH optima of 5.6–8.5, and the specific activity in our study was 45-fold higher [25]. Moreover, our data on the metal requirements of hNMNAT-1 and hNMNAT-2 identified that the two enzymes exhibited a differential requirement for magnesium ions. Calcium was found to partially activate hNMNAT-2, while hNMNAT-1 was highly activated by nickel and zinc; however, these two metal ions showed marginal and no activation, respectively, of hNMNAT-2.

In the present study, Northern blot analyses showed a highly restricted distribution of hNMNAT-2 in brain, heart and muscle. The expression of hNMNAT-2 showed one band in brain (5.6 kb) and heart tissues, but two bands (5.6 and 3.2 kb) in skeletal muscle tissue. This expression pattern could be related to the special sensitivity of these tissues to oxidative damage and NAD^+ depletion, which is linked to cell death in the heart and brain in animal models [44–46]. In mice, up-regulation of the orthologue of hNMNAT-1 protects neurons against Wallerian degeneration in response to injury such as transection and vincristine toxicity [20,21]. Thus one potential role of hNMNAT-2 may be to preserve the viability of myocardial and brain cells subjected to hypoxic injury. These data can also explain the clinical observations of neurological side effects with tiazofurin [5].

Mutation of either of two invariant amino acids, His-24 or Trp-92, resulted in catalytically inactive enzymes. Previous studies showed that mutation of the conserved histidine in the NMNAT cloned from *Methanobacterium thermoautotrophicum* (His-19 in that sequence) resulted in an inactive enzyme [15]. Crystal structures of *Methanobacterium* and human NMNAT show that the conserved His-24 nearly contacts the NAD phosphate bonded to nicotinamide ribose, and may be involved in the catalytic mechanism. The recent publication of the crystal structure of hNMNAT-1 shows important contacts of Trp-92 with the nicotinamide carbonyl and a ribose hydroxyl. Our results suggest that the contacts between the amino acid side chain and the substrate observed with the complexed crystal structure of human NMNAT are catalytically important.

To further characterize the role of hNMNAT-2 in brain, a human brain multiple-tissue Northern blot was performed. hNMNAT-2 showed strong expression in all cortical and subcortical structures as a single band of approx. 5.6 kb whereas two transcripts of 6.6 and 4.8 kb were reported in thalamus, hippocampus, corpus callosum, cordate nucleus and amygdala in the previous study [25]. However, we found that expression of hNMNAT-2 was very low in medulla, and appeared to be absent from spinal cord tissue, whereas hNMNAT-1 is predominantly expressed in the spinal cord. This was a surprising finding, considering the common developmental origin of the brain and spinal tissue.

Since NAD depletion was shown to decrease ATP and GTP pools, causing depletion of pancreatic β-cells leading IDDM [47], we examined the expression of hNMNAT-2 in the sections of human pancreas and compared the expression in sections of pancreas from three patients with insulinoma. Insulinoma is a rare pancreatic cancer in which there is proliferation of hyper-insulin-secreting cancer cells. In the exocrine parenchyma, hNMNAT-2 protein expression was weak, whereas it was strongly expressed in the islets of Langerhans. The expression was more intense in some islet cells compared with others. We have not yet been able to localize this increased expression to the β-cells. However, the peripheral location of the more intense expression is consistent with the general location of β-cells within human islets. The sections of pancreas from insulinoma patients showed strong cytoplasmic expression of hNMNAT-2 proteins similar to that seen in the islet cells. This further supports the idea of a high level of hNMNAT-2 expression in β-cells. Because pancreatic β-cells are

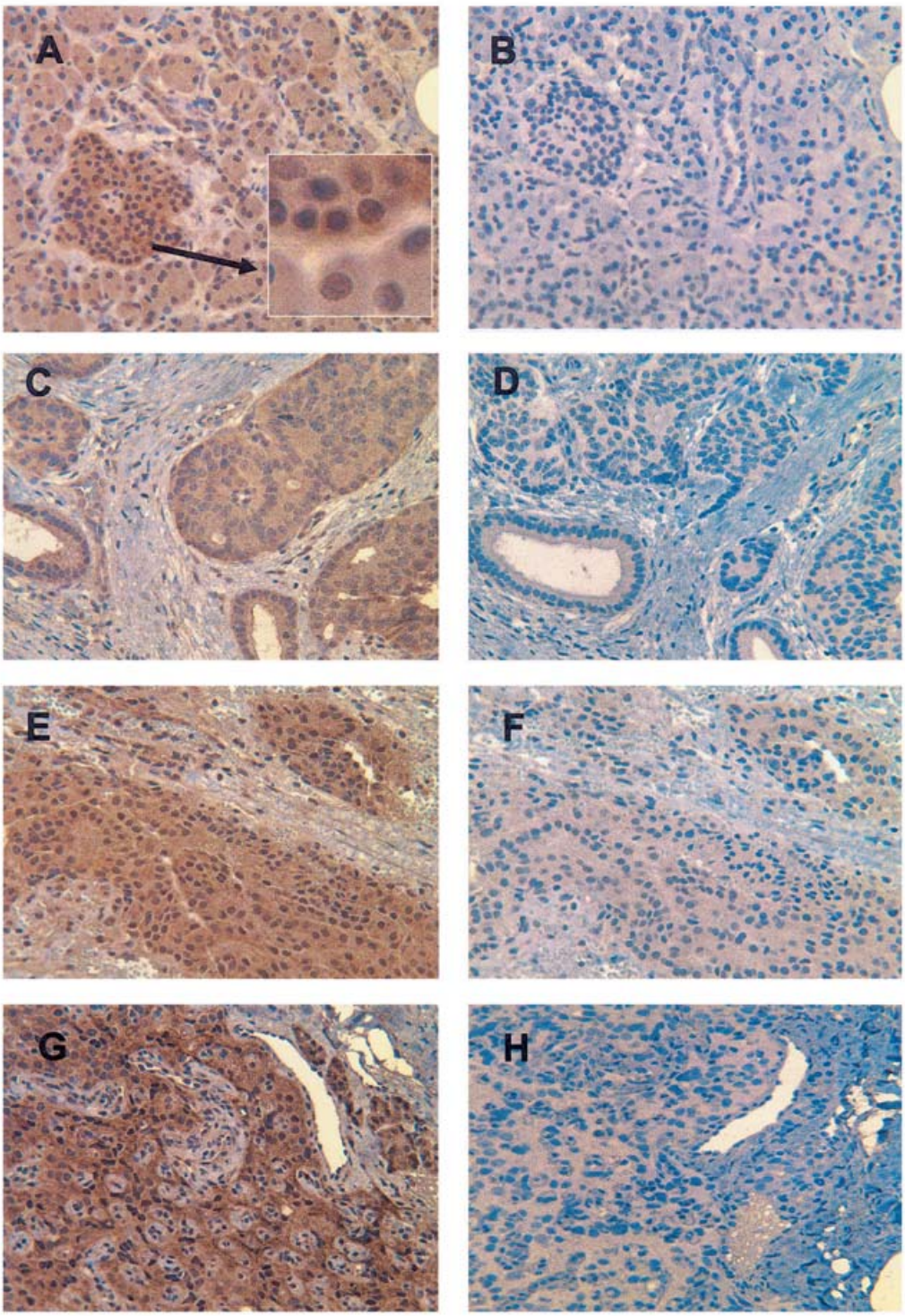

Figure 6 Immunostaining of hNMAT-2 in normal adult human pancreas and pancreas from adult insulinoma patients

Immunohistochemical staining with primary rabbit anti-hNMNAT-2 peptide IgG (**A**, normal adult pancreas; **C**, **E** and **G**, pancreas from three adult insulinoma patients, diagnosed by clinical and histological evidence) and control sections stained with non-immune rabbit serum IgG (**B**, normal pancreas; **D**, **F** and **H**, pancreas from three adult insulinoma patients) is shown at high-power magnification ($\times$ 32). (**A**, inset) Higher magnification ($\times$ 80) of peripheral Langerhans cells wherein expression of hNMNAT-2 is seen in the cytoplasm.

very sensitive to NAD depletion, expression of the hNMNAT-2 isoform may help in increasing the chances of survival of these cells.

Thus the immunohistochemical staining studies presented here show differential expression of hNMNAT-2 protein. The fact that our anti-peptide antibodies were raised against hNMNAT-2

epitopes that had no homology with hNMNAT-1 also indicates that this protein is expressed in several tissues. These studies suggest that tissues that are particularly at risk of hypoxic damage are probably protected by expression of NMNAT. The functional significance of each isoform within a given tissue remains to be elucidated.

We thank Kimberlie Milton, Tia Harvey and Srilakshmi Alagharu for excellent technical assistance. We thank Dr John Hawes for insightful discussion and encouragement. We thank Professor Roger W. Roeske for the synthesis of hNMNAT peptides. J. A. Y. was supported by a Cancer Biology Training Program Fellowship (Indiana University Cancer Center, Indiana University School of Medicine, Indianapolis, IN, U.S.A.). A. C. A. and H. N. J. were supported in part by National Institutes of Health grants R01CA58919 and R01HD39295 and a Veterans Affairs Merit Review Award.

REFERENCES

1 Garavaglia, S., D'Angelo, I., Emanuelli, M., Carnevali, F., Pierella, F., Magni, G. and Rizzi, M. (2001) Structure of human NMN adenylyltransferase: a key nuclear enzyme for NAD homeostasis. J. Biol. Chem. **277**, 8524–8530

2 Cooney, D. A., Jayaram, H. N., Gebeyehu, G., Betts, C. R., Kelley, J. A., Marquez, V. E. and Johns, D. G. (1982) The conversion of 2-beta-D-ribofuranosylthiazole-4-carboxamide to an analogue of NAD with potent IMP dehydrogenase-inhibitory properties. Biochem. Pharmacol. **31**, 2133–2136

3 Zhou, T., Kurnasov, O., Tomchick, D. R., Binns, D. D., Grishin, N. V., Marquez, V. E., Osterman, A. L. and Zhang, H. (2002) Structure of human nicotinamide/nicotinic acid mononucleotide adenylyltransferase. Basis for the dual substrate specificity and activation of the oncolytic agent tiazofurin. J. Biol. Chem. **277**, 13148–13154

4 Jayaram, H. N., Zhen, W. and Gharehbaghi, K. (1993) Biochemical consequences of resistance to tiazofurin in human myelogenous leukemic K562 cells. Cancer Res. **53**, 2344–2348

5 Jayaram, H. N., Lapis, E., Tricot, G., Kneebone, P., Paulik, E., Zhen, W., Engeler, G. P., Hoffman, R. and Weber, G. (1992) Clinical pharmacokinetic study of tiazofurin administered as a 1-hour infusion. Int. J. Cancer **51**, 182–188

6 Magni, G., Emanuelli, M., Amici, A., Raffaelli, N. and Ruggieri, S. (1997) Purification of human nicotinamide-mononucleotide adenylyltransferase. Methods Enzymol. **280**, 241–247

7 Rogozin, I. B., Kochetov, A. V., Kondrashov, F. A., Koonin, E. V. and Milanesi, L. (2001) Presence of ATG triplets in 5′ untranslated regions of eukaryotic cDNAs correlates with a 'weak' context of the start codon. Bioinformatics **17**, 890–900

8 Emanuelli, M., Carnevali, F., Lorenzi, M., Raffaelli, N., Amici, A., Ruggieri, S. and Magni, G. (1999) Identification and characterization of YLR328W, the *Saccharomyces cerevisiae* structural gene encoding NMN adenylyltransferase. Expression and characterization of the recombinant enzyme. FEBS Lett. **455**, 13–17

9 Emanuelli, M., Amici, A., Carnevali, F., Raffaelli, N. and Magni, G. (2003) Identification and characterization of a second NMN adenylyltransferase gene in *Saccharomyces cervisiae*. Protein Expression Purif. **27**, 357–364

10 Denicola-Seoane, A. and Anderson, B. M. (1990) Studies of NAD kinase and NMN:ATP adenylyltransferase in *Haemophilus influenzae*. J. Gen. Microbiol. **136**, 425–430

11 Emanuelli, M., Carnevali, F., Saccucci, F., Pierella, F., Amici, A., Raffaelli, N. and Magni, G. (2001) Molecular cloning, chromosomal localization, tissue mRNA levels, bacterial expression, and enzymatic properties of human NMN adenylyltransferase. J. Biol. Chem. **276**, 406–412

12 Mehl, R. A., Kinsland, C. and Begley, T. P. (2000) Identification of the *Escherichia coli* nicotinic acid mononucleotide adenylyltransferase gene. J. Bacteriol. **182**, 4372–4374

13 Olland, A. M., Underwood, K. W., Czerwinski, R. M., Lo, M. C., Aulabaugh, A., Bard, J., Stahl, M. L., Somers, W. S., Sullivan, F. X. and Chopra, R. (2002) Identification, characterization, and crystal structure of *Bacillus subtilis* nicotinic acid mononucleotide adenylyltransferase. J. Biol. Chem. **277**, 3698–3707

14 Raffaelli, N., Emanuelli, M., Pisani, F. M., Amici, A., Lorenzi, T., Ruggieri, S. and Magni, G. (1999) Identification of the archaeal NMN adenylyltransferase gene. Mol. Cell. Biochem. **193**, 99–102

15 Saridakis, V., Christendat, D., Kimber, M. S., Dharamsi, A., Edwards, A. M. and Pai, E. F. (2001) Insights into ligand binding and catalysis of a central step in NAD^+ synthesis. Structure of *Methanobacterium thermoautotrophicum* NMN adenylyltransferase complexes. J. Biol. Chem. **276**, 7225–7232

16 Sestini, S., Jacomelli, G., Pescaglini, M., Micheli, V. and Pompucci, G. (2000) Enzyme activities leading to NAD synthesis in human lymphocytes. Arch. Biochem. Biophys. **379**, 277–282

17 Sood, R., Bonner, T. I., Makalowska, I., Stephan, D. A., Robbins, C. M., Connors, T. D., Morgenbesser, S. D., Su, K., Faruque, M. U., Pinkett, H. et al. (2001) Cloning and characterization of 13 novel transcripts and the human RGS8 gene from the 1q25 region encompassing the hereditary prostate cancer (HPC1) locus. Genomics **73**, 211–222

18 Werner, E., Ziegler, M., Lerner, F., Schweiger, M., Muller, Y. A. and Heinemann, U. (2002) Crystallization and preliminary X-ray analysis of human nicotinamide mononucleotide adenylyltransferase (NMNAT). Acta Crystallogr. D Biol. Crystallogr. **58**, 140–142

19 Wang, M., Wu, Y., Culver, D. G. and Glass, J. D. (2001) The gene for slow Wallerian degeneration (Wld(s)) is also protective against vincristine neuropathy. Neurobiol. Dis. **8**, 155–161

20 Wang, M. S., Fang, G., Culver, D. G., Davis, A. A., Rich, M. M. and Glass, J. D. (2001) The WldS protein protects against axonal degeneration: a model of gene therapy for peripheral neuropathy. Ann. Neurol. **50**, 773–779

21 Coleman, M. P., Conforti, L., Buckmaster, E. A., Tarlton, A., Ewing, R. M., Brown, M. C., Lyon, M. F. and Perry, V. H. (1998) An 85-kb tandem triplication in the slow Wallerian degeneration (Wlds) mouse. Proc. Natl. Acad. Sci. U.S.A. **95**, 9985–9990

22 Conforti, L., Tarlton, A., Mack, T. G., Mi, W., Buckmaster, E. A., Wagner, D., Perry, V. H. and Coleman, M. P. (2000) A Ufd2/D4Cole 1e chimeric protein and overexpression of Rbp7 in the slow Wallerian degeneration (WildS) mouse. Proc. Natl. Acad. Sci. U.S.A. **97**, 11377–11382

23 Fernando, F. S., Conforti, L., Tosi, S., Smith, A. D. and Coleman, M. P. (2002) Human homologue of a gene mutated in the slow Wallerian degeneration (C57BL/Wld(s)) mouse. Gene **284**, 23–29

24 Vagnozzi, R., Marmarou, A., Tavazzi, B., Signoretti, S., Di Pierro, D., del Bolgia, F., Amorini, A. M., Fazzina, G., Sherkat, S. and Lazzarino, G. (1999) Changes of cerebral energy metabolism and lipid peroxidation in rats leading to mitochondrial dysfunction after diffuse brain injury. J. Neurotrauma **16**, 903–913

25 Raffaelli, N., Sorci, L., Amici, A., Emanuelli, M., Mazzola, F. and Magni, G. (2002) Identification of a novel human adenylyltransferase. Biochem. Biophys. Res. Commun. **297**, 835–840

26 Seki, N., Ohira, M., Nagase, T., Ishikawa, K., Miyajima, N., Nakajima, D., Nomura, N. and Ohara, O. (1997) Characterization of cDNA clones in size-fractionated cDNA libraries from human brain. DNA Res. **4**, 345–349

27 Adams, M. D., Kerlavage, A. R., Fleischmann, R. D., Fuldner, R. A., Bult, C. J., Lee, N. H., Kirkness, E. F., Weinstock, K. G., Gocayne, J. D., White, O. et al. (1995) Initial assessment of human gene diversity and expression patterns based upon 83 million nucleotides of cDNA sequence. Nature (London) **377**, 3–174

28 Altschul, S. F., Madden, T. L., Schaffer, A. A., Zhang, J., Zhang, Z., Miller, W. and Lipman, D. J. (1997) Gapped BLAST and PSI-BLAST: a new generation of protein database search programs. Nucleic Acids Res. **25**, 3389–3402

29 Balducci, E., Emanuelli, M., Raffaelli, N., Ruggieri, S., Amici, A., Magni, G., Orsomando, G., Polzonetti, V. and Natalini, P. (1995) Assay methods for nicotinamide mononucleotide adenylyltransferase of wide applicability. Anal. Biochem. **228**, 64–68

30 Fisher, C. L. and Pei, G. K. (1997) Modification of a PCR-based site-directed mutagenesis method. Biotechniques **23**, 570–574

31 Bradford, M. M. (1976) A rapid and sensitive method for the quantitation of microgram quantities of protein utilizing the principle of protein-dye binding. Anal. Biochem. **72**, 248–254

32 Letondal, C. A. (2001) Web interface generator for molecular biology programs in Unix. Bioinformatics **17**, 73–82

33 Cleland, W. W. (1979) Statistical analysis of enzyme kinetic data. Methods Enzymol. **63**, 103–138

34 Page, R. D. M. (1996) TREEVIEW: an application to display phylogenetic trees on personal computers. Comput. Appl. Biosci. **12**, 357–358

35 Kozak, M. (1991) An analysis of vertebrate mRNA sequences: intimations of translational control. J. Cell Biol. **115**, 887–903

36 Raffaelli, N., Lorenzi, T., Amici, A., Emanuelli, M., Ruggieri, S. and Magni, G. (1999) *Synechocystis* sp. slr0787 protein is a novel bifunctional enzyme endowed with both nicotinamide mononucleotide adenylyltransferase and 'Nudix' hydrolase activities. FEBS Lett. **444**, 222–226

37 Emanuelsson, O., Nielsen, H., Brunak, S. and von Heijne, G. (2000) Predicting subcellular localization of proteins based on their N-terminal amino acid sequence. J. Mol. Biol. **300**, 1005–1016

38 Milanesi, L., Muselli, M. and Arrigo, P. (1996) Hamming-Clustering method for signals prediction in 5′ and 3′ regions of eukaryotic genes. Comput. Appl. Biosci. **12**, 399–404

39 Leslie, R. G. D. and Elliott, R. B. (1994) Early environmental events as a cause of IDDM. Evidence and implications. Diabetes **43**, 843–850

40 Saravia, F. E., Revsin, Y., Gonzalez Deniselle, M. C., Gonzalez, S. L., Roig, P., Lima, A., Homo-Delarche, F. and De Nicola, A. F. (2002) Increased astrocyte reactivity in the hippocampus of murine models of type 1 diabetes; the nonobese diabetic (NOD) and streptozotocin-treated mice. Brain Res. **13**, 345–353

41 Gonzalez, C., Menissier De Murcia, J., Janiak, P., Bidouard, J. P., Beauvais, C., Karray, S., Garchon, H. J. and Levi-Strauss, M. (2002) Unexpected sensitivity of nonobese diabetic mice with a disrupted poly(ADP-ribose) polymerase-1 gene to streptozotocin-induced and spontaneous diabetes. Diabetes **51**, 1470–1476

42 Skaper, S. D. (2003) Poly(ADP-ribose)polymerase-1 in acute neuronal death and inflammation: a strategy for neuroprotection. Ann. N.Y. Acad. Sci. **993**, 217–228

43 Masutani, M., Suzuki, H., Kamada, N., Watanabe, M., Ueda, O., Nozaki, T. and Sugimura, T. (1999) Poly(ADP-ribose)polymerase gene disruption conferred mice resistant to streptozotocin-induced diabetes. Proc. Natl. Acad. Sci. U.S.A. **96**, 2301–2304

44 Cuzzocrea, S., Chatterjee, P. K., Mazzon, E., Dugo, L., Serraino, I., Britti, D., Mazzullo, G., Caputi, A. P. and Thiemermann, C. (2002) Pyrrolidine dithiocarbamate attenuates the development of acute and chronic inflammation. Br. J. Pharmacol. **135**, 496–510

45 Cuzzocrea, S., McDonald, M. C., Mazzon, E., Dugo, L., Serraino, I., Threadgill, M., Caputi, A. P. and Thiemermann, C. (2002) Effects of 5-aminoisoquinolinone, a water-soluble, potent inhibitor of the activity of poly (ADP-ribose) polymerase, in a rodent model of lung injury. Biochem. Pharmacol. **63**, 293–304

46 McDonald, M. C., Mota-Filipe, H., Wright, J. A., Abdelrahman, M., Threadgill, M. D., Thompson, A. S. and Thiemermann, C. (2000) Effects of 5-aminoisoquinolinone, a water-soluble, potent inhibitor of the activity of poly (ADP-ribose) polymerase on the organ injury and dysfunction caused by haemorrhagic shock. Br. J. Pharmacol. **130**, 843–850

47 Li, G., Segu, V. B. G., Rabaglia, M. E., Luo, R.-H., Kowluru, A. and Metz, S. A. (1998) Prolonged depletion of guanosine triphosphate induces death of insulin-secreting cells by apoptosis. Endocrinology **139**, 3752–3762

Received 4 April 2003/17 September 2003; accepted 29 September 2003
Published as BJ Immediate Publication 29 September 2003, DOI 10.1042/BJ20030518